THE EUROPEAN
PHYSICAL JOURNAL D

Regular Article – Ultraintense and Ultrashort Laser Fields

Dipole instability in molecules irradiated by XUV pulses

D. Hughes[1] , D. Dundas[1,a] , P. M. Dinh[2] , M. Vincendon[2] , P.-G. Reinhard[3] , and E. Suraud[2]

[1] School of Mathematics and Physics, Queen's University Belfast, University Road, Belfast BT7 1NN, UK
[2] Laboratoire de Physique Théorique, CNRS, UPS, Université de Toulouse, 31062 Toulouse Cedex, France
[3] Institut für Theoretische Physik, Universität Erlangen, 91058 Erlangen, Germany

Abstract. We study the response of small covalent molecules to XUV laser pulses. The theoretical description relies on a real-time and real-space Time-Dependent Density Functional Theory (TDDFT) approach at the level of the local density approximation complemented by an efficient self-interaction correction. We observe the development of a dipole instability well after the laser pulse has died out. We find that this instability mechanism is robust with respect to ionic motion, to a wide variety of laser characteristics and to the inclusion of incoherent correlations at the level of a relaxation time ansatz. To rule out any potential numerical effects, we use two independent computational implementations of the TDDFT approach. A comparison of the various laser parameters together with the widely used model approach consisting in an instantaneous hole excitation shows the generic character of this instability in terms of the level depletion of a deep lying electron state. An experimental verification of the phenomenon is proposed in terms of a time-resolved measurement of the photoelectron spectrum.

1 Introduction

The availability of ultrashort laser pulses in the XUV to X-ray frequency regime has triggered an impressive development of Ultra-Fast (UF) processes in molecules and clusters [1,2]. The great flexibility in pulse shaping as well as the possibility of accessing very short pulse durations in the attosecond regime opens the door to fully time-resolved measurements down to the electronic timescale [3]. High photon energies also give a way to explore direct electronic excitation of deeply lying states. This allows various relaxation processes to be triggered, for example Auger decay [4], charge migration in covalent molecules [5,6], interatomic (or intermolecular) Coulomb decay [7], or giant autoionization resonances in high harmonic generation [8,9].

From the theoretical point of view, a fully detailed treatment of UF excitation and relaxation remains challenging [10]. To simplify the modeling, it is often assumed that the UF pulse instantaneously removes a bound electron [11,12], even a possibly deeply bound one. This represents a major step in simplification since one overlooks details of the excitation process, while the target hole state can be chosen deliberately. Such an approach is routinely used to explore the dynamics of charge migration and charge transfer in molecular systems [13–20].

The aim of this paper is to explore in some detail the excitation processes induced by a short XUV pulse.

The excitation is explicitly simulated by an interaction of an ultrashort XUV pulse with a multi-electronic system. Both excitation and response are then studied using Time-Dependent Density Functional Theory (TDDFT) [21]. The number of active electrons is restricted thanks to the use of frozen core pseudopotentials [22,23] which, nevertheless, allows us to focus on the depletion of the lowest occupied valence state, easily attainable with an XUV laser. While low-frequency pulses skim electrons from the Fermi surface, deeper lying electron states come increasingly into play with increasing laser frequency [24–26]. This generally leads to an equi-distribution of depletion among the valence states, for example in Na clusters [24,25] and for C_{60} [26].

However, it was found recently that under certain circumstances, a properly tuned XUV pulse can deliver an ionization mechanism very close to the instantaneous creation of an instantaneous deep-hole [27]. This generates an occupation inversion where energy can be released by filling the deep lying hole with an electron from much less depleted higher lying levels. A remarkable consequence of the ensuing de-excitation of the system is the appearance of a dipole instability with a delayed reappearance of the dipole signal well after the pulse is over and the original dipole signal has died out. The thus reappearing dipole oscillations lead to further electron emission leaving as a footprint a marked low-energy peak in a photoelectron spectrum which could be used for experimental identification of the process. It was checked in Ref. [27] that this dipole instability

a e-mail: d.dundas@qub.ac.uk (corresponding author)

remains active if dynamical correlations from electron–electron collisions are included (handled within a relaxation time ansatz (RTA) [28]). Such a scenario bears some similarities with a revival mechanism in quantum optics observed for a two-level system coupled to photon modes and often modeled with the Jaynes-Cummings Hamiltonian [29]. The present case differs in that we deal with an open system because electrons can be emitted and in that we use a mean-field approximation in which the dipole oscillations are not quantized. While we observe a revival of dipole oscillations, we never see multiple collapses/revivals.

In order to further explore the many open issues the present manuscript thus continues systematic investigations of the dipole instability with different molecules, a broader variety of photon pulse parameters, and including ionic motion. The aim here is to validate the robustness of the instability mechanism in a wide variety of dynamical setups. This will provide a set of relevant cases for future investigations on the origin and quantitative details of this mechanism.

2 Theoretical background

The calculations presented in this paper have been carried out using two separate computer packages, QDD (Quantum Dissipative Dynamics) [30] and EDAMAME (Ehrenfest DynAMics on Adaptive MEshes) [31], both of which solve the time-dependent Kohn-Sham (TDKS) equations of TDDFT using different numerical approaches. In both packages, we work at the level of the Local Density Approximation (LDA) [32] with the functional of [33]. We refer to this approach as the time-dependent LDA (TDLDA). To access a proper dynamical treatment of ionization, we need a realistic description of single particle (s.p.) energies. For this purpose, we add a Self-Interaction Correction (SIC) [34]. The simple and efficient average-density SIC (ADSIC) [35–38] is our choice here.

We shall consider here two small covalent molecules as test cases, the nitrogen dimer N_2 and acetylene C_2H_2. Results for these two molecules have been generated using two implementations of real time TDDFT, namely QDD [30] and EDAMAME [31]. The use of these different packages allows us to safeguard against potential numerical artifacts in the observed dipole instabilities. The main aspects of each package are briefly discussed in the Appendix. In the remainder of this section, we give a brief description of the laser pulses used in the calculations, together with a discussion of how various observables are calculated.

2.1 Laser pulse

The two molecules considered here are excited by an XUV pulse which is described as a classical (coherent), linearly polarized photon field. We shall consider both polarizations with respect to the molecular axis (both N_2 and C_2H_2 are linear): along the molecular axis, here-

after labeled "longitudinal polarization" or z, and perpendicular to it, hereafter labeled "transverse polarization" or xy. For a longitudinal polarization, the corresponding potential reads:

$$V_{\text{pulse}} = eE_0 z \, f(t) \cos \left[\omega_{\text{XUV}}(t - T_{\text{pulse}}) \right] \qquad (1a)$$

$$f(t) = \begin{cases} \sin^2 \left(\pi \dfrac{t}{2T_{\text{pulse}}} \right) & t \in \{0, \, 2T_{\text{pulse}}\} \\ 0 & \text{otherwise} \end{cases} \qquad (1b)$$

The pulse parameters are: frequency ω_{XUV}, duration T_{pulse}, and field strength E_0 (related to the pulse intensity as $I \propto E_0^2$).

In the following, we focus on XUV pulses. Frequencies lie around $\omega_{\text{XUV}} \sim 50$ eV for both N_2 and C_2H_2. This is the frequency domain in which the observed deep level depletion with subsequent instability is particularly strong. In our first exploration, we used a short pulse with $T_{\text{pulse}} = 1$ fs and adjusted the laser intensity so that the total ionization N_{esc} levels off asymptotically at about one. Typical intensities were of the order of 10^{15} W/cm^{-2}. This comes close to the scenarios modeled by an instantaneous full hole. Here, we will explore a wider range of pulse profiles, lower intensities (down to a few 10^{13} W/cm^{-2}) and/or longer pulse durations (up to 30 fs). Lower intensities will reduce the amount of level depletion. The interesting question is whether this still creates an occupation inversion, i.e. a situation where the lowest level is more depleted than the higher ones, and whether the dipole instability again appears under the varied circumstances.

2.2 Observables

The analysis of the dynamics is based on three observables that describe both the dipole response and ionization. The first one is the time evolution of the dipole moment

$$\mathbf{D}(t) = e \int \mathrm{d}^3\mathbf{r} \, \mathbf{r} \, \varrho(\mathbf{r}, t) \qquad (2)$$

where the single electron density is computed as

$$\varrho(\mathbf{r}) = \sum_\alpha w_\alpha(t) |\varphi_\alpha(\mathbf{r}, t)|^2 \qquad (3)$$

where $\varphi_\alpha(\mathbf{r}, t)$ is the time-dependent s.p. wave function of state α and $w_\alpha(t)$ is its occupation number. The summation over α deserves a word of comment. It runs on all computed states. In TDLDA calculations, only occupied states are treated and have $w_\alpha = 1$, independent of time. At RTA level, the w_α's become dynamical and take fractional time-dependent values [28,30].

The optical response is attained by delivering an initial small kick. The dipole signal is then recorded in time and analyzed with spectral methods [39]. The optical response characterizes the dynamical response of a system to a laser and is thus the entry door to the system's dynamical response.
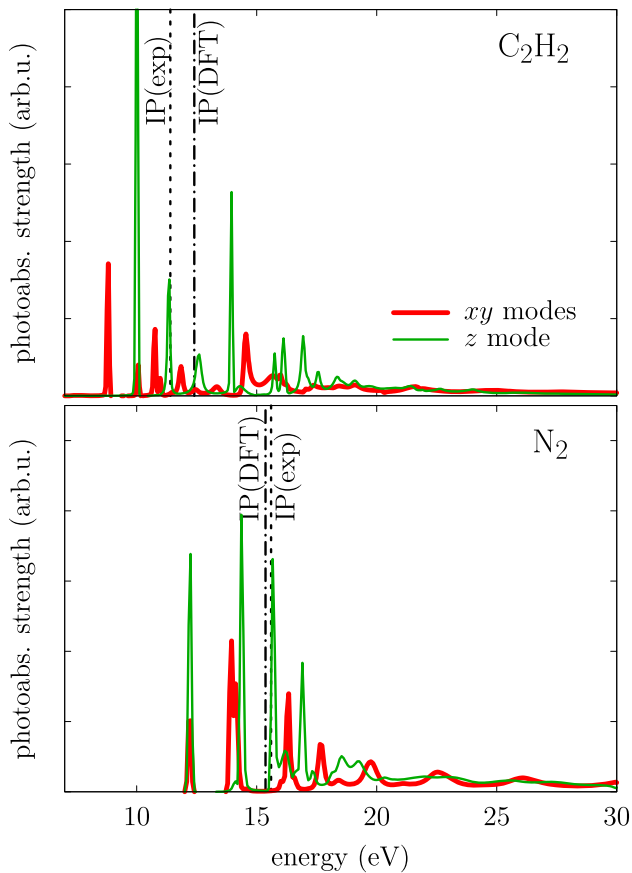
Fig. 1 Photoabsorption spectra of the C_2H_2 (upper) and N_2 molecules (lower) along the molecular axis (z direction) and the transverse plane (xy plane). The experimental and theoretical ionization potentials (IP) are indicated by dotted and dashed-dotted vertical lines respectively. Note that the theoretical result is the vertical IP (no rearrangement of ions) while the experimental value stands for the adiabatic IP

The optical response (or photoabsorption spectrum) of our two test molecules N_2 and C_2H_2 are shown in Fig. 1. The ionic distance of N_2 is taken as 2.02 a_0 (the experimental value is 2.08 a_0), which represents the minimum of the Born-Oppenheimer surface for our setup (pseudopotential and ADSIC). This gives the occupied single particle states having the following energies: $\varepsilon_{2\sigma_g} = -32.5$ eV, $\varepsilon_{2\sigma_u} = -18.6$ eV, $\varepsilon_{1\pi_u} = -17.7$ eV, $\varepsilon_{3\sigma_g} = -15.1$ eV (the experimental values are -37.3 eV, -18.6 eV, -16.6 eV, and -15.5 eV, respectively). For C_2H_2 the C–H bond length is 2.07 a_0 (experimental value: 2.00 a_0) and the C–C bond length 2.29 a_0 (experimental value: 2.27 a_0). This gives the occupied single particle states having the following energies: $\varepsilon_{2\sigma_g} = -23.5$ eV, $\varepsilon_{2\sigma_u} = -17.8$ eV, $\varepsilon_{3\sigma_g} = -15.5$ eV, $\varepsilon_{1\pi_u} = -11.5$ eV (the experimental values are -23.6 eV, -18.8 eV, -16.7 eV, and -11.4 eV, respectively). As usual in covalent systems, the optical responses display a fragmented spectral distribution, here with a few peaks below the Ionization Potential (IP) and a widely spread contribution in the continuum. Figure 1 displays optical responses up to 30 eV where the signals die out. This means that for XUV frequencies of ~ 50 eV, as used in this work, no resonance with any mode will occur.

The second observable is the electron content n_α of each s.p. wave function, associated to its complement, the depletion $\bar{n}_\alpha$:

$$n_\alpha(t) = w_\alpha \int d^3\mathbf{r}\, |\varphi_\alpha(\mathbf{r},t)|^2 \ , \ \overline{n}_\alpha(t) = 1 - n_\alpha(t) \tag{4}$$

The total number of "escaped" electrons, i.e. total ionization, is then simply obtained as

$$N_{\text{esc}}(t) = \sum_\alpha \overline{n}_\alpha(t) = N - \sum_\alpha n_\alpha(t) \tag{5}$$

where N is the initial number of computed electrons (10 for N_2 and C_2H_2).

The last observable of interest, especially for experimental access, is the Photo-Electron Spectrum (PES). We evaluate it here with the simple and efficient method of [40–42]: the time evolution of each s.p. wave function is recorded at several measuring points shortly before the absorbing boundaries begin. The signal is then Fourier transformed to energies which provides the spectrum of kinetic energies of the escaping electrons, that is the PES. In the case of strong fields, an additional phase correction has to be added [43].

3 Results

3.1 Ultra fast XUV pulses

In [27], we reported the appearance of a dipole instability in N_2 following irradiation by an ultrafast (UF) laser pulse in the frequency range around $\omega_{\text{XUV}} \sim 50$ eV. This feature is of a general nature and can be found in many other systems. We exemplify that by extending the investigation to another covalent molecule, namely acetylene (C_2H_2). Figure 2 recalls the basic impression of the dipole instability. It shows the dipole response to a 1 fs XUV pulse with wavelength $\lambda = 27$ nm ($\omega_{\text{XUV}} = 45.97$ eV), intensity $I = 5 \times 10^{15}$ W/cm^2 and laser polarization along the molecular (z) axis. The dipole signal is plotted in linear scale here to demonstrate its initial extinction and seemingly sudden reappearance much later.

The effect is surprising at first glance. It is clear that the intense photon pulse leaves considerable energy in the molecule. One expects that this is quickly distributed over internal degrees of freedom and never comes back. But it comes back coherently, collected into one visible dipole oscillation. The mechanism behind this was explained in [27]: the XUV pulse cuts a hole into a deep lying s.p. state which constitutes a metastable configuration. The energy stored in the
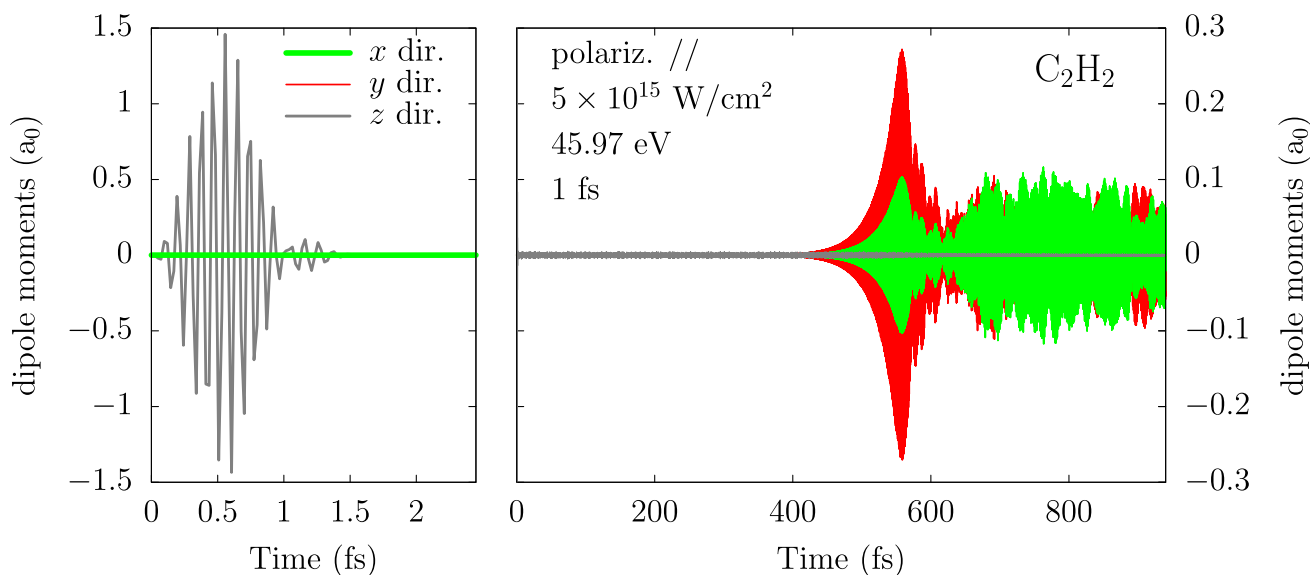
Fig. 2 Dipole moments in x, y and z directions for acetylene interacting with a linearly polarized laser pulse of wavelength $\lambda = 27$ nm (ω_{XUV}= 45.97 eV), peak intensity $I = 5\times10^{15}$ W/cm^2, pulse duration $T_{pulse} = 1$ fs, and laser polarization aligned to molecular (z) axis. Short times are displayed in the left panel to make the immediate dipole response to the laser pulse visible, while the right panel shows the time evolution at longer times removing the signal for the first 2 fs)

hole is discharged predominantly into one particular particle-hole oscillation, in this case between the hole state $2\sigma_g$ and the HOMO $2\pi_u$. The oscillation builds up with exponentially increasing amplitude. Figure 2 shows the dipole instability growing in the x and y directions as opposed to along the laser polarization direction as we previously observed in [27]. This is because the instability can manifest itself in different components of the dipole depending on system and initial condition. Up to about 600 fs, the D_x and D_y signal move strictly in phase (not visible at plotting resolution). These initial oscillations move actually along a line in the x-y plane oriented 70° relative to the D_x axis. Later on, further modes come into play and the components run out of phase. The initial direction is, in principle, arbitrary because C$_2$H$_2$ is an axially symmetric system. The triaxial numerical representation leaves a faint symmetry violation which eventually sets the initial direction. Furthermore, it is important to note that the initial growth up to 600 fs oscillates with a unique frequency of 13.4 eV which is composed from the $2\pi_u \leftrightarrow 2\sigma_g$ energy difference of 12 eV plus the contribution from the Coulomb residual interaction. We observe this feature in all examples of dipole instability. Its frequency is thus predominantly a systems property.

While Fig. 2 shows the dipoles on a linear scale, they can be visualized better on a logarithmic scale. Figure 3 presents, on a logarithmic scale, the dipole response to a 1 fs XUV pulse of wavelength $\lambda = 27$ nm (ω_{XUV}= 45.97 eV), polarization aligned along the molecular axis, for three intensities: $I = 4\times10^{15}$ W/cm^2, $I = 5\times10^{15}$ W/cm^2 and $I = 6\times10^{15}$ W/cm^2. Note that the time interval shown depends on the laser intensity: up to 200 fs for the highest intensity and 940 fs for the other two. At the lowest intensity, no instability occurs. At
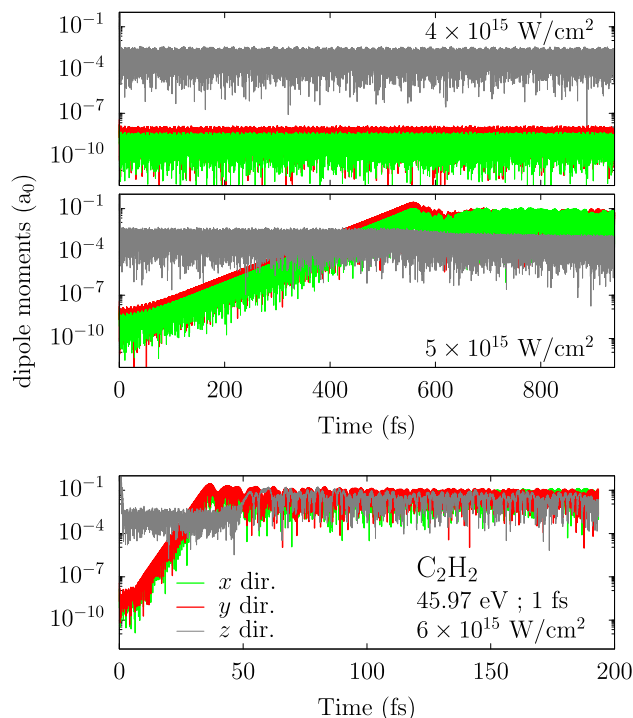

Fig. 3 Absolute dipole moments in x, y and z directions for acetylene interacting with a linearly polarized laser pulse of wavelength $\lambda = 27$ nm (ω_{XUV}= 45.97 eV), pulse duration $T_{pulse} = 1$ fs, polarization aligned with the molecular (z) axis, and three laser intensities as indicated. The dipole response is shown in a log scale to better appreciate the exponential growth of the instability. Note that the time scales are different in the two upper panels as compared to the lowest panel
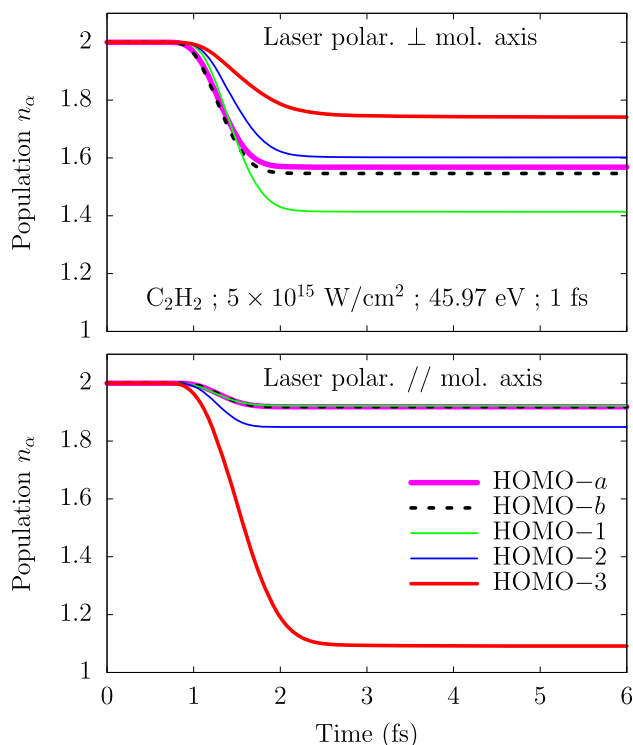
Fig. 4 Orbital populations for acetylene interacting with a linearly polarized laser pulse of wavelength $\lambda = 27$ nm ($\omega_{\mathrm{XUV}} = 45.97$ eV), laser intensity $I = 5 \times 10^{15}$ W/cm^2 and pulse duration $T_{\mathrm{pulse}} = 1$ fs. Ions are kept fixed. Both laser polarizations (longitudinal and transverse) are considered

Fig. 5 Absolute dipole moments in the x, y and z directions for acetylene interacting with a linearly polarized laser pulse of wavelength $\lambda = 27$ nm ($\omega_{\mathrm{XUV}} = 45.97$ eV), laser intensity $I = 5 \times 10^{15}$ W/cm^2, and pulse duration Tpulse $= 1$ fs. The laser polarization direction is aligned along the molecular axis. The response is compared for two situations, one in which the ions are kept fixed, the other in which the ions are allowed to move

the two higher intensities, the instability appears and the time scale for the higher intensity is shorter. The instability initially manifests itself in the dipoles along the transverse axes (x and y). At the highest intensity, we also see an increase in the dipole along the z-axis after 50 fs.

It is interesting to compare what occurs for different orientations of the laser polarization with respect to the molecular axis. We repeated the calculations presented in Fig. 3 with the laser polarization along the x-axis, i.e. perpendicular to the molecular axis. In that case, no instability occurs for the three laser intensities considered. To understand that, we have to analyze the mechanisms of hole creation by the XUV pulse for this molecule, similarly as we previously did for N$_2$ [27,44]. Figure 4 shows the occupation of the KS orbitals for the laser intensity of 5×10^{15} W/cm^2. With the pulse aligned parallel to the molecular axis, one observes a by far dominant depletion of the most deeply bound level, with only small depletion of less bound states. This is close to a case which could be simplified by drilling an instantaneous hole in the system. Recall that such an instantaneous hole creation is widely used to model UF irradiation scenarios [11,12]. We have shown previously that already this simple mechanism produces the dipole instability [44]. The situation is somewhat different when the laser polarization is aligned perpendicular to the molecular axis. There, one observes a balanced
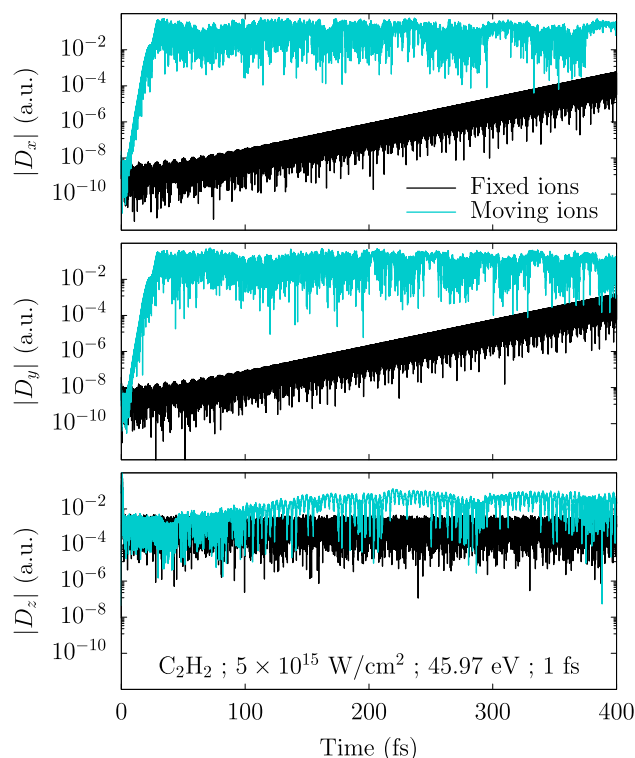
depletion of all states, the most deeply lying one being, in fact, the least depleted state. In that case, there is no deep-lying hole state which could support the instability.

In the case of N$_2$ irradiated by 1 fs pulses [27], we found that ionic motion played no role. This made sense for several reasons, namely the large nitrogen mass, the short pulse duration and because the instability occurred rather quickly once the pulse was over (below 10 fs) and thus even below the N$_2$ vibration period (around 14 fs). The results for C$_2$H$_2$ in Fig. 3 agree with these former results, to a large extent quantitatively. Still, acetylene contains hydrogen atoms with a potentially much higher mobility than nitrogen. It is thus interesting to study the impact of ionic motion in that case, all the more as we shall explore below other irradiation scenarios involving longer time scales (in section 3.2). Figure 5 compares the dipole response for both fixed and moving ions in the case of a laser polarized along the molecular axis. The laser intensity is $I = 5 \times 10^{15}$ W/cm^2 corresponding to the intensity used in the middle panel of Fig. 3. For acetylene, we see that the effect of ionic motion is dramatic. In the case of moving ions, the instability manifests itself more rapidly than in the case of fixed ions. Indeed the timescale over
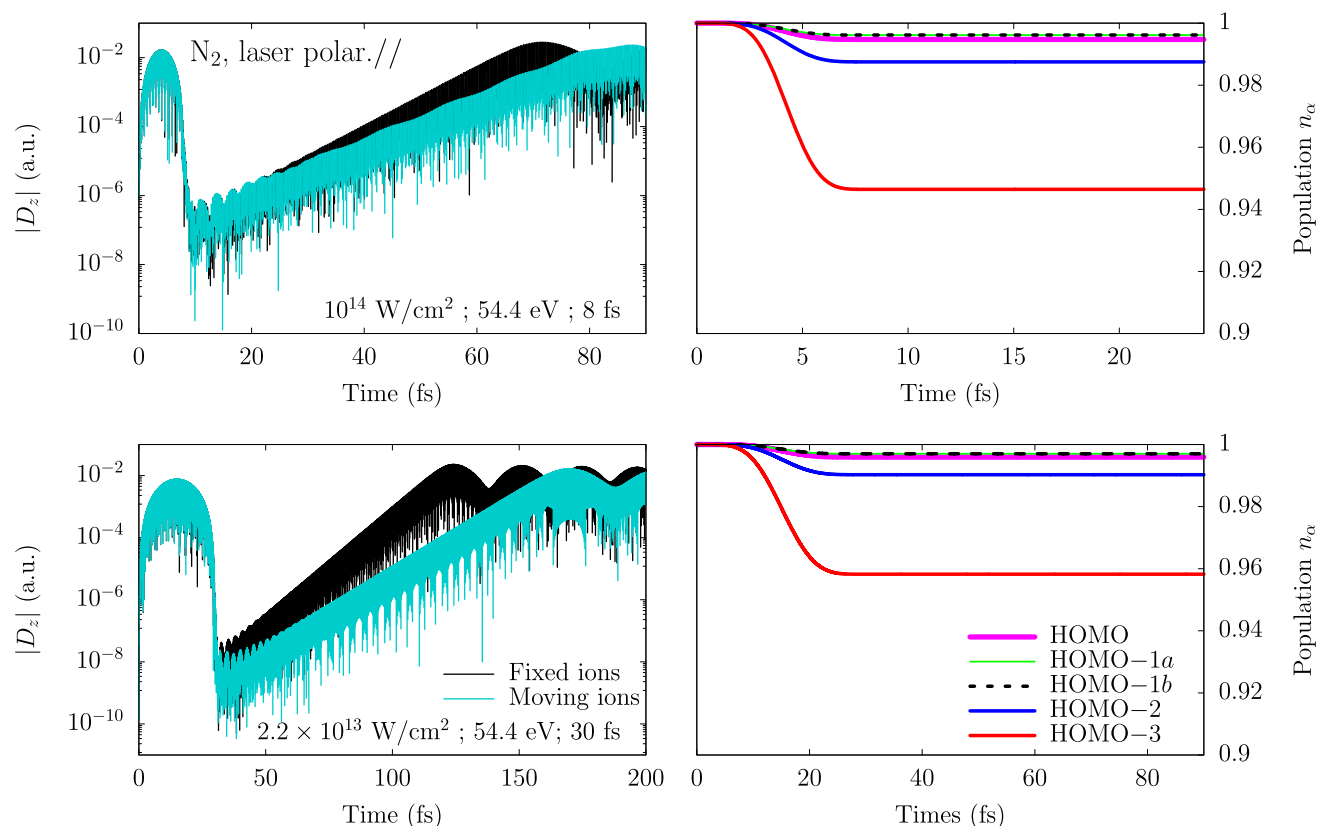
Fig. 6 Time evolution of dipole signal along laser polarization for a longitudinal excitation in N_2 and for two "long" pulses at lower laser intensity. Pulse frequency is $\omega_{XUV} = 54.4$ eV in both cases. Top panels: pulse duration T_{pulse}= 8 fs and intensity $I = 10^{14}$ W/cm^2. Bottom panels: T_{pulse}= 30 fs and intensity $I = 2.2 \times 10^{13}$ W/cm^2. Different time spans are used according to T_{pulse} Both simulations with frozen ions and moving ions are considered. The right panels show the time evolution, up to $3T_{pulses}$, of the populations which are almost identical, regardless the ionic motion treatment

which the instability develops is similar to the fixed ion simulation for a laser intensity of 6.0×10^{15} W/cm^2.

3.2 The case of longer pulses

Up to this point we have considered the following laser setups: very short pulses (1 fs), high frequencies (40-50 eV range), and rather high intensities (in the 10^{14-15} W/cm^2 range). This leads to an ionization close to unity with, in some case, nearly exact depletion of one deeply lying single electron level. Such a scenario comes close to a practical realization of an instantaneous pure hole depletion. In addition, there is a possible connection between this level depletion and the onset of the instability, as is suggested by model studies [44]. The latter investigations furthermore suggest that instability may occur for partial depletion of low lying states. It is thus interesting to explore whether this may be achieved by considering other laser conditions. The phase space of laser parameters is huge (polarization, frequency, duration, intensity mostly). We already investigated the role of frequency in [27] and found that deep-level depletion emerges only in limited frequency intervals which depend on the system. They remain, for the examples of N_2 and C_2H_2, in the frequency range 50 ± 10 eV. We

shall focus here on the effect of varying the pulse duration and intensity. Both are not independent of each other as decreasing intensity reduces energy deposit and ionization (subsequently depletion) which can be compensated by considering longer pulses.

We scanned a large variety of intensities and pulse lengths for a laser frequency $\omega_{XUV} = 54.4$ eV irradiating N_2. The occupation inversion (largest depletion in the lowest valence state) appears under any condition. But the subsequent dipole instability requires a minimum amount of depletion. Two results for N_2 just above instability threshold are shown in Fig. 6, namely (i) pulse duration $T_{pulse} = 8$ fs and intensity $I = 1.0 \times 10^{14}$ W/cm^2 (upper panels) and (ii) pulse duration $T_{pulse} = 30$ fs and intensity $I = 2.2 \times 10^{13}$ W/cm^2 (lower panels). In both cases, the laser polarization is longitudinal and the dipole signal is plotted in longitudinal direction as well. The excitation energy is 5.0 eV for case (i) and 4.1 eV for case (ii) and the depletions are 0.11 and 0.10 respectively (out of total ionization of 0.13 and 0.10 respectively) therefore much less than typical ionization of one in previous test cases [27] and in the C_2H_2 example above. Again, the instability builds up very neatly in both cases, starting from a vanishing dipole signal after the pulse up to an amplitude of about
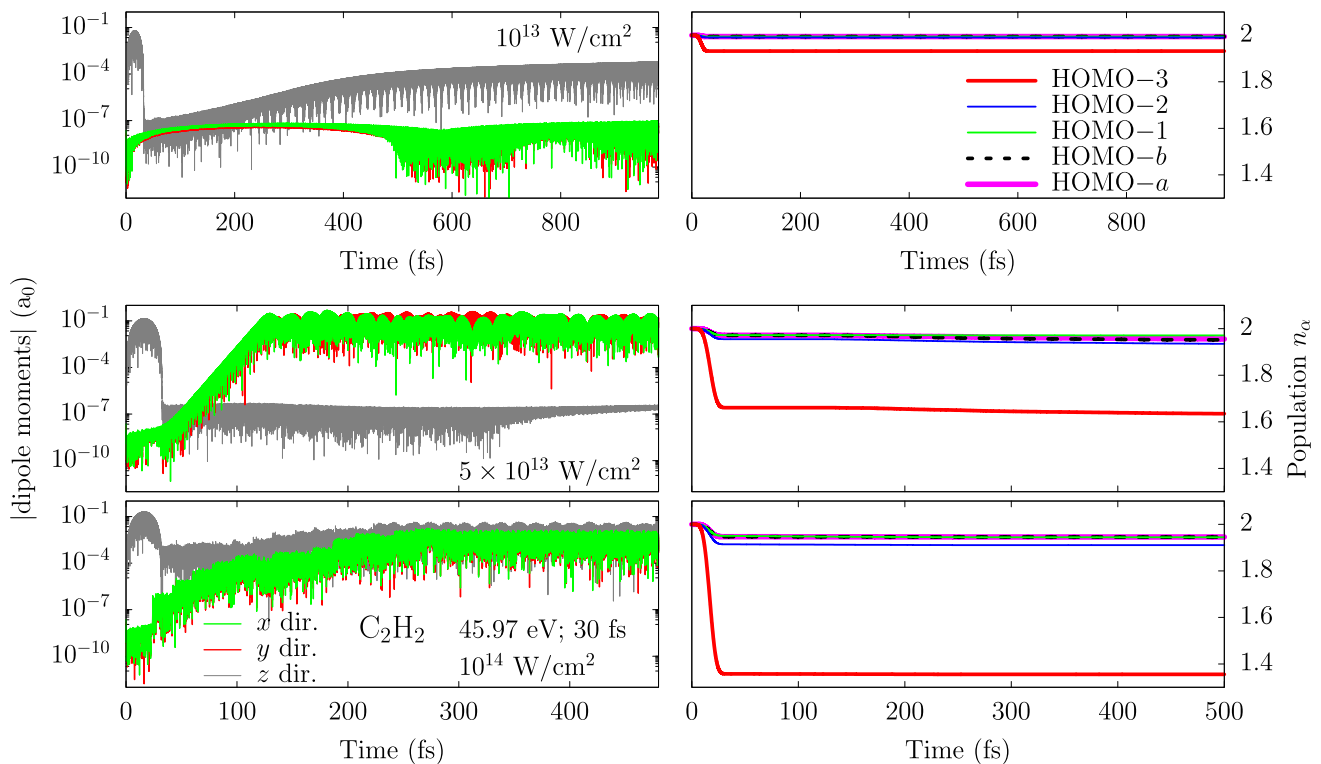
Fig. 7 Absolute dipole moments in the x, y and z directions for acetylene interacting with a linearly polarized laser pulse of wavelength $\lambda = 27$ nm ($\omega_{\mathrm{XUV}} = 45.97$ eV), pulse duration $T_{\mathrm{pulse}} = 30$ fs and various laser intensities as indicated. In these simulations the ions are allowed to move

0.01 asymptotically. However, the much smaller excitation and depletion causes much longer times scales for growth of the instability (the systematic trend will be discussed in connection with Fig. 9).

The rather long time scales for these two test cases call for the inclusion of ionic motion. Figure 6 thus shows results with and without ionic motion. The difference is visible, but still small for the 8 fs pulse, and becomes a quantitative issue for the longer 30 fs pulse. However, the appearance of the dipole instability as such remains unaffected by ionic motion in both cases. The level populations (right panels) decrease in time and quickly level off after $\gtrsim T_{\mathrm{pulse}}$. Since the effect of ionic motion is only visible well after the laser is off, ionic motion does not impact at all the time evolution of the level populations.

It is also interesting to study the onset of instability for the case of long pulses in a systematic way, e.g., by varying laser intensity. An example is shown in Fig. 7 for C_2H_2 for moderate laser intensities in the 10^{13-14} W/cm^2 range, while keeping the same pulse duration at 30 fs. The laser polarization is longitudinal (along the z axis). The results presented here show the same qualitative behavior as those for short pulses shown in Fig. 3. In particular, as the laser intensity increases, the instability grows faster. Indeed, for the highest intensity, we see the instability already developing in the immediate aftermath of the pulse. The right panels of Fig. 7 show the time evolution of level populations as complemen-

tary information. As in the N_2 case discussed above, the final depletion is practically reached at the end of the laser pulse. Also for the long pulse used here, we see that depletion of the deepest state prevails and that it grows, naturally, with increasing intensity. The result suggests a direct relation between the amount of depletion and the growth rate of the dipole signal (left panels). This link had also be found in studies with short pulses and with instantaneous hole excitation. Looking very carefully at the right panels, we see a faint additional depletion at about 200 fs. This is the shake-off induced by the re-appearing dipole oscillations which, however, has no effect on the overall trends.

In the case of UF pulses in N_2, we outlined a way how the dipole instability could be observed experimentally in a simple manner by considering the PES. The dipole oscillations caused by the instability produce a marked low energy peak in the PES, well separated from the peaks connected to the XUV frequency [27]. For the 1 fs cases, the instability pops up rather rapidly (within less than 10 fs) which makes measuring a time-resolved PES rather challenging. In the case of longer pulses, as explored here, the situation is more forgiving as the instability evolves on much longer time scales. It is thus interesting to check what a PES looks like in such scenarios. An example is presented in Fig. 8 for the case of N_2 irradiated by a 30 fs pulse at intensity $I = 2.2 \times 10^{13}$ W/cm^2. The PES is computed at early and long times. The early time window (up to 30 fs)
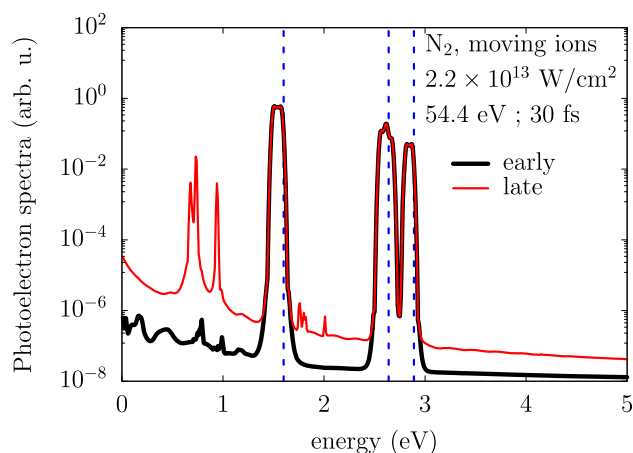
Fig. 8 PES at early (up to 30 fs) and late (up to 210 fs) times for N_2 irradiated by a $\omega_{XUV} = 54.4$ eV laser pulse of duration $T_{pulse}= 30$ fs and intensity 2.2×10^{13} W/cm^2 with moving ions. The vertical dashes indicate the single particle energies of the HOMO, HOMO-1 and HOMO-2 shifted by ω_{XUV}

corresponds to the end of the laser pulse. As visible in Fig. 6, the instability has not set yet in and the PES therefore delivers the expected pattern with peaks positioned at the single particle energies shifted by ω_{XUV} (see vertical dashes). The late time window (up to 210 fs) includes the development of the instability and its subsequent extra ionization that leads to a modification of the PES at low energy. As in the case of N_2 with a 1 fs pulse [27], this low energy peak cannot be attributed to any combination of laser frequency and single particle energies. Furthermore, it is only visible at late times. It can hence only be attributed to the dipole instability itself. The present case is very similar to the example of a short pulse of [27] and it explores the same spectral range. We find again that the location of the low energy peak (around 10 eV) reasonably matches the Ionization Potential (IP $\simeq 16.2$ eV at late time) plus twice the instability frequency (here $\omega_{instab}=14.4$ eV). More studies are necessary to develop more quantitative conclusions. It is also to be noted that the similarity of the PES holds although the present case of a long pulse was computed with ionic motion and the previous case of a short pulse without. To be on the safe side, we counter-checked the present case with frozen ions and find that ionic motion does not change the position of the low energy peak.

3.3 Discussion

The above examples have shown that a great variety of laser setups lead to a dipole instability, independent on pulse intensity or duration. The original case of UF pulses in N_2 [27] is not accidental as we observe similar patterns in C_2H_2. Such instability scenarios seem to be related to sufficient population inversion, or depletion of the lowest state respectively. This is confirmed by calculations using an instantaneous hole in the deepest level
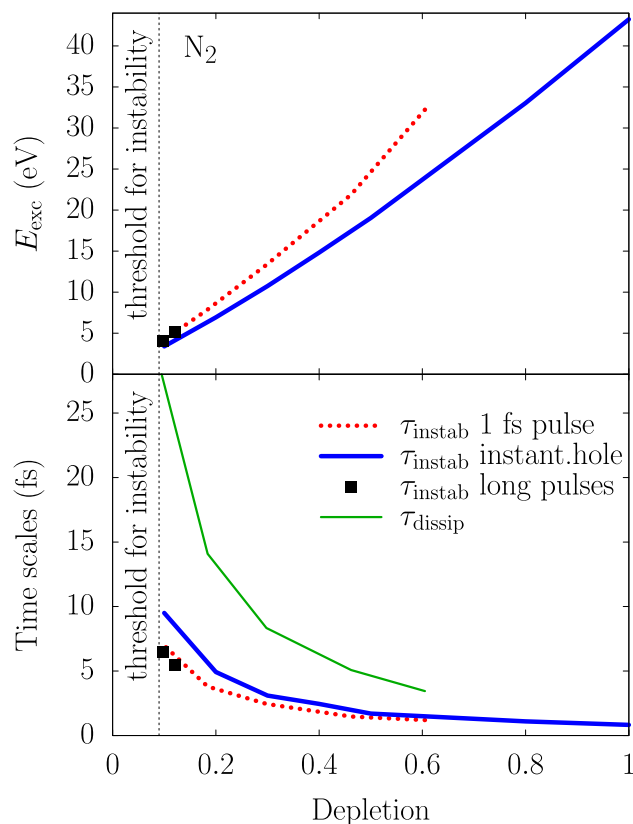

Fig. 9 Excitation energy (top) and time scales (bottom) as functions of depletion for the N_2 dimer. Excitation mechanisms are: (i) 1 fs pulse at $\omega_{XUV} = 58$ eV (red dots), (ii) initialization by an instantaneous hole in the lowest level (blue thick line) complemented by (iii) long pulses from Fig. 6 (squares). In the lower panel, the time scales are τ_{instab}, the time within which the dipole signals grows by a factor e, and τ_{dissip} (green thin line), the time of reduction of the dipole signal through RTA dissipation

as an initial condition, and the effect persists for different amounts of depletion [44], which bears some similarity the various scenarios we have investigated here. It is thus interesting to try to summarize our results using depletion of the lowest valence state as a guideline. Figure 9 shows such a summary. The figure gathers two major excitation mechanisms: i) the one by a short (1 fs) XUV pulse of $\omega_{XUV} = 58$ eV (red line); ii) the one by an instantaneous hole in the lowest level (blue line) as explored in [44]. The pulse intensity of the 1 fs pulse has been varied to produce a series of depletions. The two above excitation mechanisms are complemented by the two results from the long pulses shown in Fig. 6, as indicated by filled black squares. The lower panel of Fig. 9 displays the most relevant times at play, namely τ_{instab}, the time within which the dipole signals grows by a factor e, and τ_{dissip}, the time of reduction of the dipole signal through dissipation as described in RTA [28]. We have seen above that ionic motion does not play a key role here and omitted those results in the figure.

Figure 9 displays several interesting features. The first aspect can be seen in the upper panel of the figure. It shows the relation between excitation energy (read off after electron emission from the 1 fs pulse is over and before the instability starts new electron emission) and depletion. The relation is close to linear and the 1 fs pulse cases behave very close to the pure hole model mechanism in this respect. The second aspect concerns the evolution of time scales with level depletion or alternatively (see upper panel) deposited excitation energy. Times decrease with excitation energy or level depletion and again instability times τ_{instab} of 1 fs pulses and pure hole behave quite similarly. RTA times also strongly depend on excitation energy, namely $\propto E_{\mathrm{exc}}$ [28]. But, importantly for our purpose is the fact that the RTA time τ_{dissip} always lies much above the instability time τ_{instab} by typically a factor 2 at high excitation/depletion and up to a factor of 3 at low excitation/depletion. This implies that incoherent dynamical correlations, as modeled at the RTA level, cannot efficiently compete with the instability and are unable to prevent it from appearing. It does not mean, though, that the RTA would have no effect. In fact, on the longer term, it will damp out dipole oscillations efficiently [28] and thus play a decisive role on the long term behavior of the system. But on the "short" times associated to the onset of instability, RTA does not hinder it and only reduces the final oscillation amplitude quantitatively [27].

Two last remarks are finally to be made on Fig. 9. The first one concerns the vertical line labeled "threshold of instability". It primarily refers to the systematic investigations performed using direct hole depletion (no laser) as explored in [44]. It was observed there that the instability did not develop for depletion below a certain threshold which lies somewhere below a depletion of 0.1, associated to a threshold excitation energy of about 4 eV. Interestingly enough the closeness between the 1 fs laser pulse and the direct hole scenarios is confirmed by direct UF laser computations in which too small an intensity leads to no instability. Even more interesting is the fact that the same holds true when considering longer pulses at low intensity as explored in section 3.2. The two cases for N_2 shown in Fig. 6 are indicated as squares in Fig. 9. In both depletion/excitation energy and depletion/times plots, the values furthermore remarkably match the systematic values obtained with 1 fs pulses. This strengthens the statement that details of the laser setup seem unimportant, as seen with 1 fs pulses compared to direct hole excitation.

4 Conclusion

We explored in this paper the response of two small covalent molecules, namely C_2H_2 and N_2, to XUV laser pulses of various characteristics. We started with ultrafast pulses tuned to remove 1 electron from the system, a setup which matches the model excitation mechanism consisting in instantaneously creating a hole in

a system, an approach widely used in ultrafast science. We observed that such a short XUV pulse leads to a dipole instability, well after the pulse is over. The effect is robust, independent of numerical details, which we have further checked by using two different real-time and real-space TDDFT codes. It is also robust with respect to ionic motion, even in a molecule containing very mobile hydrogen atoms. Laser polarization can make a difference in detail. But the dipole instability can take place for any polarization in connection with the appropriate laser frequency. At a qualitative level, we can conclude that the dipole instability is a robust effect which can appear for a great variety of conditions.

For more quantitative insights, we explored different laser setups thereby focusing on the XUV frequency range around 50 eV which we had identified as optimal for producing the instability [27]. Varying the laser intensity, we find that the dipole instability persists down to rather weak pulses until the average ionization drops down to about 1/10 electron below which the instability is absent. The growth rate of the instability depends sensitively on the depletion of the lowest valence orbital which, in turn, depends on laser intensity. The lower the intensity, the lower the rate, or the longer the growth time. We also varied the laser pulse length up 30 fs and found that the instability remains robust, which makes it more accessible to fs lasers. However, ionic motion has to be considered at those times scales. We checked and found that ionic motion may change the instabilities growth rate quantitatively, but does not lead to a qualitative change of the picture.

Besides laser parameters, we checked the impact of dynamical correlations (many-body effects beyond TD-LDA). As with ionic motion, they can change dipole amplitudes and time scales quantitatively. However, within the studies we had carried out so far, they do not overrule the dipole instability as a principal effect.

A possible experimental verification of the dipole instability could be achieved by time-resolved photoelectron spectra (PES) measurements. While on short times after the laser pulse, the PES is exhibiting only peaks related to the XUV frequency, low energy peaks develop at later times, once the instability has become manifest and the amplitude of the associated dipole mode has become large enough to produce an extra ionization visible on the PES. We have shown here that the analysis in terms of time-resolved PES remains also applicable to long pulses which brings such an experiment close to feasibility.

Author contributions

DH and DD carried out calculations using EDAMAME. P-GR, PMD, MV and ES carried out calculations using QDD. All authors contributed equally to the analysis of results and the preparation of the manuscript.

Declarations

Conflict of interest The authors declare that they have no conflict of interest.

Appendix

TDLDA and RTA within QDD

QDD solves the TDKS equations on a real-space grid. Electron emission is obtained via absorbing boundary conditions using a mask function [45,46]. Electron-ion coupling is described using Goedecker type pseudopotentials [22]. Ionic positions are treated by classical molecular dynamics or kept frozen when the time scale of the considered electronic processes is very short.

We also complement the TDLDA (+ADSIC) simulations by exploring incoherent electronic dynamical correlations at a level of the RTA [28,30,47]. A detailed description of the theory, the numerical realization in coordinate-space representation, and the actual code QDD (Quantum Dissipative Dynamics) can be found in [30].

In the cases computed in this paper, wave functions and fields are represented on a 3D grid with a grid spacing of 0.4 a_0 and 96 grid points in each direction. Stationary electronic states (ground state) are computed using an accelerated gradient method. The TDKS equa-

tions are propagated using a time-splitting technique [30,48] with a time step of 0.0006 fs.

TDLDA within EDAMAME

EDAMAME solves the TDKS equations using adaptive real-space grid techniques in 3D [31]. In the calculations presented in this paper, a global adaption is used where the position vector on the grid is scaled according to

$$\boldsymbol{r} = f(x)\boldsymbol{i} + g(y)\boldsymbol{j} + h(z)\boldsymbol{k}, \tag{6}$$

where $f(x)$, $g(y)$ and $h(z)$ are the transformation functions in the three coordinates. We use the transformations

$$f(x) = 2x + \frac{1}{2}\big[\eta(x-X_{\text{inn}}) - \eta(x+X_{\text{inn}})\big] \tag{7a}$$

$$g(y) = 2y + \frac{1}{2}\big[\eta(y-Y_{\text{inn}}) - \eta(y+Y_{\text{inn}})\big] \tag{7b}$$

$$h(z) = 2z + \frac{1}{2}\big[\eta(z-Z_{\text{inn}}) - \eta(z+Z_{\text{inn}})\big] \tag{7c}$$

$$\eta(\xi) = \xi\,\text{erf}(\xi) + \frac{e^{-\xi^2}}{\sqrt{\pi}} \tag{7d}$$

where X_{inn}, Y_{inn} and Z_{inn} denotes a transition point between an inner and outer region in x, y and z respectively. The effect of this transformation is to give regular grid spacing that doubles when going from the inner to the outer region. The transition point is set to 10 a_0 for all coordinates with the inner region grid spacing set to 0.2 a_0 (i.e. increasing to 0.4 a_0 in the outer region). Along each coordinate we use 275 grid points which gives a grid extent of ±44.8 a_0. All differential operators in the TDKS equations are approximated using 5-point central difference formula.

Electron-ion interactions are described using norm-conserving Troullier-Martins pseudopotentials [23] in their fully-separable Kleinman-Bylander form [49]. As with QDD, ionic positions are either treated by classical molecular dynamics or kept frozen.

Stationary electronic states are computed using a Chebyshev Filtered Subspace Iteration method [50]. The TDKS equations are then propagated using an 18th-order Arnoldi propagation scheme with a time step of 0.00242 fs [31]. This scheme is supplemented by the predictor-corrector scheme outlined in [30] in order to improve energy conservation. Electron emission is described via absorbing boundary conditions using a mask function [31].

References

1. F. Krausz, M. Ivanov, Rev. Mod. Phys. **81**, 163 (2009)
2. Y. Linda et al., J. Phys. B: At. Mol. Opt. Phys. **51**, 032003 (2018)
3. F. Calegari, G. Sansone, S. Stagira, C. Vozzi, M. Nisoli, J. Phys. B: At. Mol. Opt. Phys. **49**, 110 (2016)

4. K. Ueda, E. Sokell, S. Schippers, F. Aumayr, H. Sadegh-pour, J. Burgdorfer, C. Lemell, X.M. Tong, T. Pfeifer, F. Calegari, A. Palacios, Roadmap on photonic, electronic and atomic collision physics: I. Light-matter interaction. J. Phys. B: At. Mol. Opt. Phys. **52**(17), 171001 (2019). https://doi.org/10.1088/1361-6455/ab26d7

5. A. Marciniak, V. Despré, V. Loriot, G. Karras, M. Hervé, L. Quintard, F. Catoire, C. Joblin, E. Constant, A.I. Kuleff, F. Lépine, Nat. Commun. **10**, 337 (2019)

6. H.J.B. Marroux, A.P. Fidler, A. Ghosh, Y. Kobayashi, K. Gokhberg, A.I. Kuleff, S.R. Leone, D.M. Neumark, Nat. Commun. **11**, 5810 (2020)

7. T. Jahnke, U. Hergenhahn, B. Winter, R. Dörner, U. Frühling, P.V. Demekhin, K. Gokhberg, L.S. Ceder-baum, A. Ehresmann, A. Knie, A. Dreuw, Chem. Rev. **120**, 11295 (2020)

8. I.S. Wahyutama, T. Sato, K.L. Ishikawa, Phys. Rev. A **99**, 063420 (2019)

9. Dane R. Austin, Allan S. Johnson, Felicity McGrath, David Wood, Lukas Miseikis, Thomas Siegel, Peter Hawkins, Alex Harvey, Zdenek Masin, Serguei Patchkovskii, Morgane Vacher, Joao Pedro, Malhado, Misha Y. Ivanov, Olga Smirnova, and Jon P. Marangos, *Sci. Rep.*, 11, 2485 (2021)

10. M. Ruberti, Phys. Chem. Chem. Phys. **21**, 17584 (2019)

11. L.S. Cederbaum, W. Domcke, J. Schirmer, W. Von Niessen, Adv. Chem. Phys. **65**, 115 (1986)

12. L.S. Cederbaum and, J. Zobeley. Chem. Phys. Lett. **307**, 205 (1999)

13. R. Weinkauf, P. Schanen, A. Metsala, E.W. Schlag, M. Buergle, H. Kessler, J. Phys. Chem. **100**, 18567 (1996)

14. F. Remacle, R.D. Levine, E.W. Schlag, R. Weinkauf, J. Phys. Chem. A **103**, 10149 (1999)

15. F. Remacle, R.D. Levine, Proc. Natl. Acad. Sci. **103**, 6793 (2006)

16. A.I. Kuleff, L.S. Cederbaum, Phys. Rev. Lett. **106**, 053001 (2011)

17. A.I. Kuleff, N.V. Kryzhevoi, M. Pernpointner, L.S. Cederbaum, Phys. Rev. Lett. **117**, 093002 (2016)

18. N.V. Golubev, J. Vaníček, A.I. Kuleff, Phys. Rev. Lett. **127**, 123001 (2021)

19. C.E.M. Gonçalves, R.D. Levine, F. Remacle, Phys. Chem. Chem. Phys. **23**, 12051 (2021)

20. Attosecond charge migration following oxygen K-shell ionization in DNA bases and base pairs. Phys. Chem. Chem. Phys. 23, 23005, (2021)

21. E. Runge, E.K.U. Gross, Phys. Rev. Lett. **52**, 997 (1984)

22. S. Goedecker, M. Teter, J. Hutter, Phys. Rev. B **54**, 1703 (1996)

23. N. Troullier, J.L. Martins, Phys. Rev. B **43**, 1993 (1991)

24. S. Vidal, Z.P. Wang, P.M. Dinh, P.-G. Reinhard, E. Suraud, Frequency dependence of level depletion in na clusters and in c_2h_4. J. Phys. B: At. Mol. Opt. Phys. **43**, 165102 (2010)

25. P.M. Dinh, S. Vidal, P.-G. Reinhard, E. Suraud, Fingerprints of level depletion in photoelectron spectra of small na clusters in the uv domain. New J. Phys. **14**, 063015 (2012)

26. C.-Z. Gao, P. Wopperer, P.M. Dinh, E. Suraud, P.-G. Reinhard, On the dynamics of photo-electrons in c_{60}. J. Phys. B: At. Mol. Opt. Phys. **48**, 105102 (2015)

27. P.G. Reinhard, D. Dundas, P.M. Dinh, M. Vincen-don, E. Suraud, Unexpected dipole instabilities in small molecules after ultrafast xuv irradiation. Phys. Rev. A **107**, L020801 (2023). https://doi.org/10.1103/PhysRevA.107.L020801

28. P.-G. Reinhard, E. Suraud. Ann. Phys. (N.Y.), **354**, 183 (2015)

29. Special Issue on Jaynes-Cummings physics. J. Phys. B: At. Mol. Opt. Phys. **46**(22) (2013)

30. P.M. Dinh, M. Vincendona, F. Coppens, E. Suraud, P.-G. Reinhard, Quantum dissipative dynamics (qdd): A real-time real-space approach to far-off-equilibrium dynamics in finite electron systems. Comp. Phys. Comm. **270**, 108155 (2022)

31. D. Dundas, Multielectron effects in high harmonic generation in n_2 and benzene: Simulation using a non-adiabatic quantum molecular dynamics approach for laser-molecule interactions. J. Chem. Phys. **136**, 194303 (2012)

32. R.M. Dreizler, E.K.U. Gross, *Density functional theory: an approach to the quantum many-body problem* (Springer-Verlag, Berlin, 1990)

33. J.P. Perdew, Y. Wang, Phys. Rev. B **45**, 13244 (1992)

34. J.P. Perdew, A. Zunger, Phys. Rev. B **23**, 5048 (1981)

35. E. Fermi, E. Amaldi, Accad. Ital. Rome **6**, 117 (1934)

36. C. Legrand, E. Suraud, P.-G. Reinhard, J. Phys. B: At. Mol. Opt. Phys. **35**, 1115 (2002)

37. P. Klüpfel, P.M. Dinh, P.-G. Reinhard, E. Suraud, Phys. Rev. A **88**, 052501 (2013)

38. P.-G. Reinhard, E. Suraud, Theoret. Chem. Acc. **140**, 63 (2021)

39. F. Calvayrac, P.-G. Reinhard, E. Suraud, Spectral signals from electronic dynamics in sodium clusters. Ann. Phys. **255**, 125 (1997)

40. A. Pohl, P.-G. Reinhard, E. Suraud, Towards single particle spectroscopy of small metal clusters. Phys. Rev. Lett. **84**, 5090 (2000)

41. A. Pohl, P.-G. Reinhard, E. Suraud, Influence of intermediate states on photoelectron spectra. J. Phys. B: At. Mol. Opt. Phys. **34**, 4969 (2001)

42. P. Wopperer, P.M. Dinh, P.-G. Reinhard, E. Suraud, Phys. Rep. **562**, 1 (2015)

43. P.M. Dinh, P. Romaniello, P.-G. Reinhard, E. Suraud, Phys. Rev. A **87**, 032514 (2013)

44. Paul-Gerhard Reinhard, Phuong Mai Dinh, Daniel Dundas, Eric Suraud, and Marc Vincendon. On the stability of hole states in molecules and clusters. Eur. Phys. J. Spec. Top. (2022). https://doi.org/10.1140/epjs/s11734-022-00676-6

45. C.A. Ullrich, J. Mol. Struct. **501**−**502**, 315 (2000)

46. P.-G. Reinhard, P.D. Stevenson, D. Almehed, J.A. Maruhn, M.R. Strayer, Role of boundary conditions in dynamic studies of nuclear giant resonances. Phys. Rev. E **73**, 036709 (2006)

47. P.M. Dinh, L. Lacombe, P.-G. Reinhard, E. Suraud, M. Vincendon, Eur. Phys. J. B **91**, 246 (2018)

48. M.D. Feit, J.A. Fleck, A. Steiger, J. Comp. Phys. **47**, 412 (1982)

49. L. Kleinman, D.M. Bylander, Phys. Rev. Lett. **48**, 1425 (1982)

50. Y. Zhou, Y. Saad, M.L. Tiago, J.R. Chelikowsky, J. Comp. Phys. **219**, 172 (2006)

51. Archer2 data files. https://doi.org/10.17034/e4c4269a-3f00-4c72-b725-65f3affa957b